Chapter 8
HM Processes

Gesa Ziefle, Jobst Maßmann, Norihiro Watanabe, Dmitri Naumov, Herbert Kunz and Thomas Nagel

8.1 Fluid Injection in a Fault Zone Using Interface Elements with Local Enrichment

This section focuses on coupled hydraulic–mechanical processes in a fault zone. The presented benchmark is motivated by the "Fault Slip (FS)" experiment of the Mont Terri Project.[1] In this experiment, a fluid injection into a fault zone is carried out and the resulting hydraulic and mechanical effects are monitored. The fault zone is characterized by a range of minor and major faults and the experiment comprises several steps where various locations are influenced by an injection. More information about this experiment as well as similar approaches can be found in Guglielmi et al. (2015b), and Guglielmi et al. (2015a), and Derode et al. (04/2015).

Modelling this system is a challenging task that has been selected to be part of the DECOVALEX-2019 project[2]–where Task B focuses on related modeling approaches and their comparison.

[1] https://www.mont-terri.ch/
[2] www.decovalex.org
[3] https://docs.opengeosys.org/docs

G. Ziefle (✉) · J. Maßmann · H. Kunz
BGR, Federal Institute for Geosciences and Natural Resources, Hanover, Germany
e-mail: Gesa.Ziefle@bgr.de

N. Watanabe
National Institute of Advanced Industrial Science and Technology, Renewable Energy Research Center (AIST), Koriyama, Fukushima, Japan

D. Naumov · T. Nagel
Helmholtz Centre for Environmental Research - UFZ, Leipzig, Germany

T. Nagel
Trinity College Dublin, Dublin, Ireland

O. Kolditz et al. (eds.), *Thermo-Hydro-Mechanical-Chemical Processes in Fractured Porous Media: Modelling and Benchmarking*,
Terrestrial Environmental Sciences, https://doi.org/10.1007/978-3-319-68225-9_8

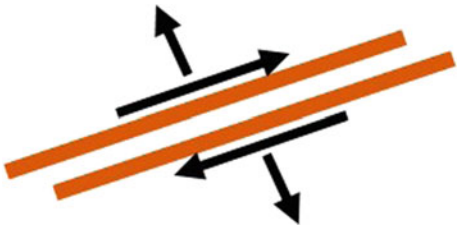

Fig. 8.1 Representation of the fracture elements in the LIE modelling approach

The following section presents a simplified 2-dimensional model approach using interface elements (LIE) of co-dimension one with local enrichment functions of the finite-element solution space to simulate the fracture behavior due to a fluid injection (for implementational details see Watanabe et al. 2012). The simulations are carried out with OpenGeoSys 6.[3] More information on modelling approaches can also be found in Rutqvist et al. (2015).

8.1.1 Model Approach

The detailed model approach is presented in Watanabe et al. (2012). It is based on the usage of lower-dimensional interface elements (LIE) for simulating flow through the fracture in combination with a Heaviside-enriched solution space to model the displacement discontinuity across the fracture. The discrete fracture is modeled by a pair of surfaces between which normal and shear displacements are permissible as presented in Fig. 8.1.

The effective-stress approach is used to calculate the stress field in the fracture:

$$\boldsymbol{\sigma}_{\mathrm{tot,f}} = \boldsymbol{\sigma}_{\mathrm{eff,f}} - \alpha_{\mathrm{f}} p_{\mathrm{f}} \mathbf{1} \tag{8.1}$$

with $\boldsymbol{\sigma}_{\mathrm{tot,f}}$ and $\boldsymbol{\sigma}_{\mathrm{eff,f}}$ being the total and effective stresses in the fracture linked via the Biot coefficient in the fracture α_{f} and the fluid pressure in the fracture p_{f}.

The relationship between the effective stress and the fracture relative displacement vector results from:

$$\mathrm{d}\boldsymbol{\sigma}_{\mathrm{eff,f}} = \mathbf{K}\,\mathrm{d}\mathbf{w} \tag{8.2}$$

with the fracture shear and normal displacements being part of the displacement vector $\mathbf{w}$, the vector of the effective stress increment defined analogously, and the stiffness matrix comprising the normal, shear and coupled stiffness of the fracture given by:

$$\mathbf{K} = \begin{bmatrix} k_{\mathrm{tt}} & k_{\mathrm{tn}} \\ k_{\mathrm{nt}} & k_{\mathrm{nn}} \end{bmatrix} \tag{8.3}$$

Concerning the fluid flow, the fracture is modeled based on the parallel-plate assumption where the fluid flow along the fracture $\mathbf{q}_{\mathrm{f}}$ is directly related to fracture aperture b_{h} by the cubic law such that:

$$\mathbf{q}_\mathrm{f} = \frac{b_\mathrm{h}^2}{12\mu_\mathrm{FR}}\mathbf{I}\,(-\nabla p_\mathrm{f} + \rho_\mathrm{FR}\mathbf{g}) \tag{8.4}$$

with the fluid viscosity μ_FR, the fluid density ρ_FR and the gravity vector $\mathbf{g}$. Assuming a uniform pressure across the fracture width, this yields to the mass balance equation:

$$b_\mathrm{h} S_\mathrm{f} \frac{\partial p_\mathrm{f}}{\partial t} + \alpha_\mathrm{f} \frac{\partial b_\mathrm{h}}{\partial t} + \nabla \cdot (b_\mathrm{h}\mathbf{q}_\mathrm{f}) + q^+ + q^- = 0 \tag{8.5}$$

with the leakage flux from the opposing fracture surfaces to the surrounding porous media q^+ and q^- and the specific storage of the fracture S_f resulting from $S_\mathrm{f} = \frac{1}{K_\mathrm{f}}$ with the compressibility of the fracture K_f and the time t.

The fracture is assumed to be characterized by elasto-plastic material behavior following the Mohr–Coulomb failure criterion. Based on the mentioned elasto–plastic behaviour, the variable fracture aperture b_h is calculated from elastic and inelastic contributions:

$$b_\mathrm{h} = b_\mathrm{h,init} + \Delta b_\mathrm{h,elastic} + \Delta b_\mathrm{h,shear} \tag{8.6}$$

with the initial fracture aperture $b_\mathrm{h,init}$, the elastic part of the aperture $b_\mathrm{h,elastic}$ (change following from Eq. (8.2)) and the opening due to the shear dilation of the fracture $b_\mathrm{h,shear}$.

8.1.2 Model Set-Up

The modeled two-dimensional domain has an extent of 20 m times 20 m as it is presented in Fig. 8.2.

The initial effective stresses are assumed to be 6 MPa in horizontal and 7 MPa in vertical direction. The pore pressure is assumed to be initially 0.5 MPa in the

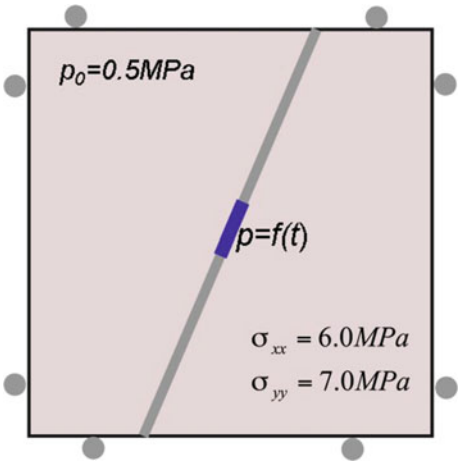

Fig. 8.2 Geometry and initial and boundary conditions of the modeled domain

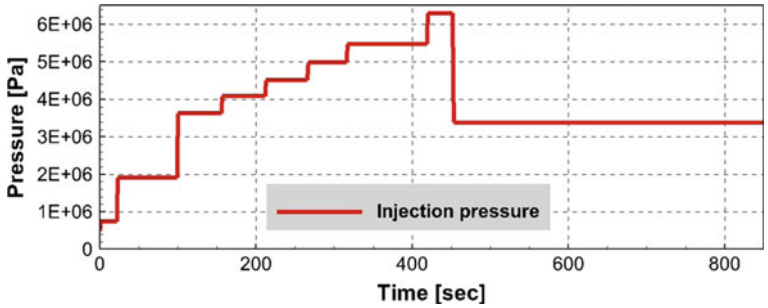

Fig. 8.3 Temporal evolution of the pressure boundary condition at the injection point

Table 8.1 Material parameters: fluid injection in a fault zone

Symbol	Parameter	Unit	Value
Host rock (elastic)			
E	Young's modulus	GPa	6.1
ν	Poisson number	–	0.3275
α_r	Biot coefficient	–	0
ρ_{SR}	Density of solid	$kg \cdot m^{-3}$	2450
ϕ	Porosity	–	0.0
K	Intrinsic permeability	m^2	1e-17
S_r	Storage	1/Pa	1.0e-10
Fault zone (elasto-plastic)			
K_n	Normal stiffness	GPa/m	20
K_s	Shear stiffness	GPa/m	20
α_f	Biot coefficient	–	1
ψ_{MC}	Dilatancy angle	deg	10
ϕ_{MC}	Friction angle	deg	22
c_{MC}	Cohesion	–	0
$b_{h,init}$	Initial fracture hydraulic aperture	m	1e-5
S_f	Storage	1/Pa	4.4e-10
Fluid			
μ_{FR}	Viscosity	$Pa \cdot s$	1e-3
ρ_{FR}	Density of water	$kg \cdot m^{-3}$	1000

entire domain and remains at this value at the model boundary. The displacements are constrained in directions normal to the boundary as indicated in Fig. 8.2. The temporal evolution of the injection pressure in the center of the model domain is presented in Fig. 8.3 and assigned as a Dirichlet boundary condition.

The material parameters are summarized in Table 8.1 and the FEM-mesh is given in Fig. 8.4.

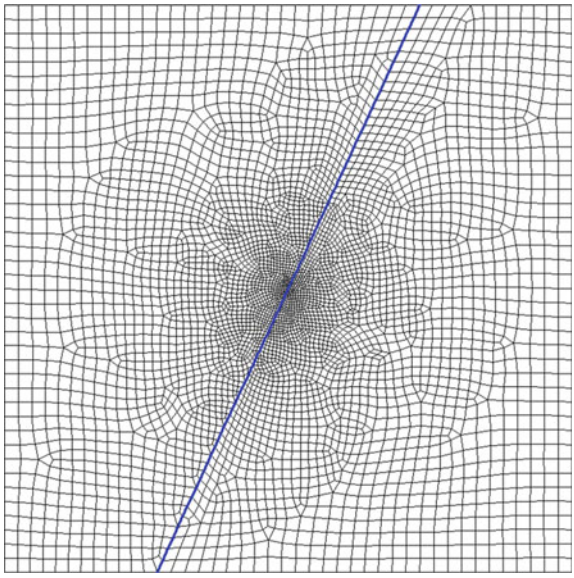

Fig. 8.4 Two-dimensional mesh and lower-dimensional representation of the fault zone

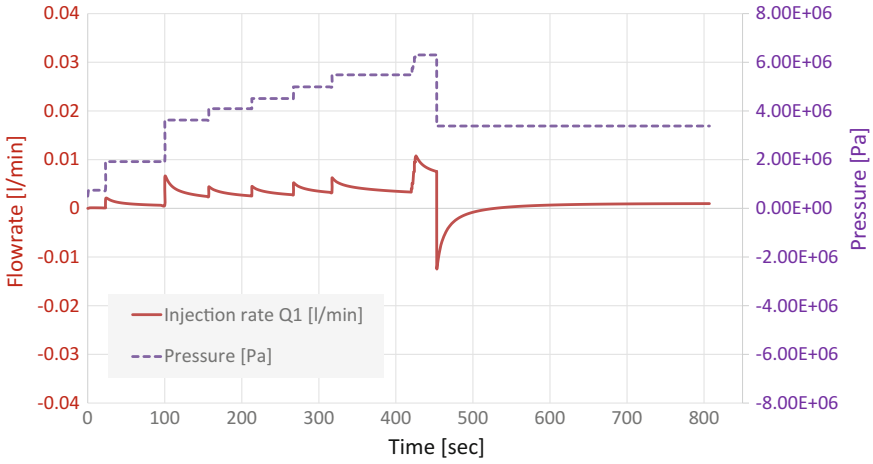

Fig. 8.5 Temporal evolution of the flowrate and the pressure in the injection point

8.1.3 Results

The injection causes significant stress redistribution in the fault zone, resulting in elasto-plastic normal as well as shear deformations due to the Mohr–Coulomb failure criterion.

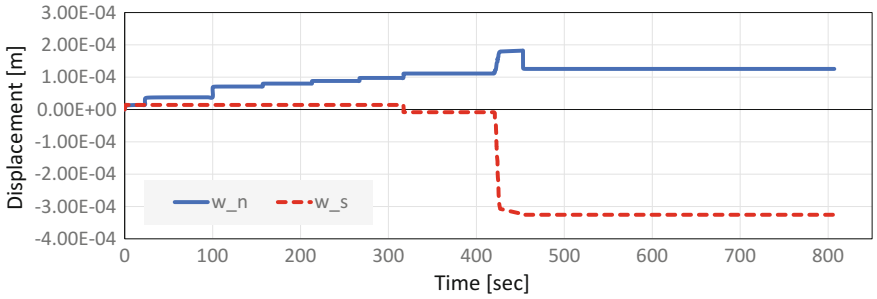

Fig. 8.6 Temporal evolutions of the normal and shear displacement of the crack in the injection point

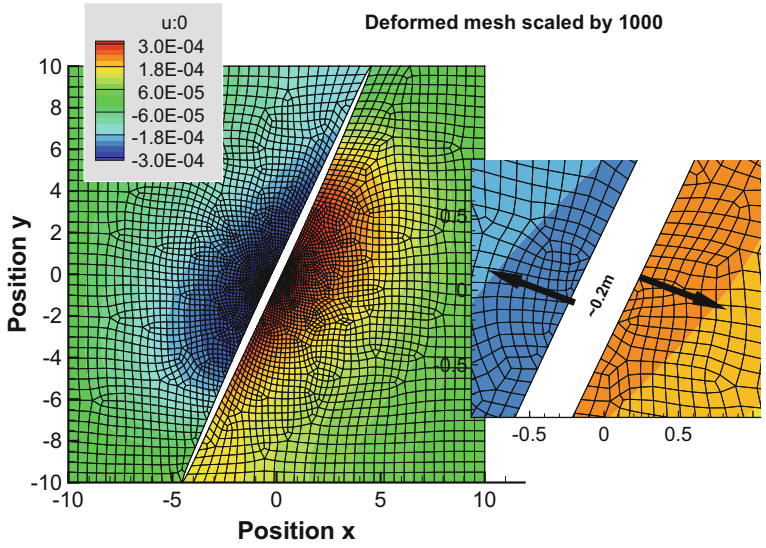

Fig. 8.7 Horizontal displacements presented as contour plot in the entire domain after 450 s at maximal injection pressure. The displaced mesh is scaled by a factor of 1000. The zoomed area indicates the shear displacements in the center of the domain. The discontinuity embodied via solution-space enrichment is clearly visible

The resulting time-dependent flowrate into the crack is presented in Fig. 8.5 in combination with the injection pressure at the injection point. The step-wise pressure increase leads to an inflow into the fault domain while the subsequently applied decrease of the injection pressure initially leads to a backflow since the pressure in the fault is higher than the injection pressure at this time step.

The temporal evolution of the normal and shear displacements of the crack in the injection point are presented in Fig. 8.6. A moderate increase of normal displacements and hardly any shear displacements can be seen during the first 420 s. After that, the

Table 8.2 Benchmark deposit (https://docs.opengeosys.org/books/bmb-5)

BM code	Author	Code	Files	CTest
BMB5-8.1	Gesa Ziefle	OGS-6	Available	ToDo

(https://oc.ufz.de/index.php/s/nlph7bhfDkj6tC7)

failure criterion is reached and a significant increase of the normal displacements due to dilatancy is accompanied by significant shear displacements. The normal displacements feature an elastic rebound due to the decrease of the injection pressure. A contour plot of the displacements at maximum injection pressure is presented in Fig. 8.7. Information about the benchmark deposit can be found in (Table 8.2).

The OGS-6 version used is available at:

- https://github.com/endJunction/ogs/tree/LIE3D_0.